2018 Annual American Control Conference (ACC)
June 27–29, 2018. Wisconsin Center, Milwaukee, USA

H_∞ Based Disturbance Observer Design for Non-minimum Phase Systems with Application to UAV Attitude Control

Ximin Lyu[1], Minghui Zheng[2], and Fu Zhang[1]

***Abstract*— This paper presents a disturbance observer (DOB) design methodology, which is applicable to both multi-input-multi-output (MIMO) and non-minimum phase systems. The DOB is designed via minimizing H_∞ norm of closed-loop dynamics from disturbance to its estimation error. This proposed design methodology returns the optimal stable plant inverse and Q filter with guaranteed closed loop stability for a given baseline feedback system, which is more efficient than manual design and tunning that involves lots of effort for either MIMO or non-minimum phase systems. Furthermore, it utilizes well-established H_∞ synthesis in robust control theory, and can be further transformed to a convex optimization problem with linear matrix inequality (LMI) constraints and solved efficiently using existing software thereafter. This design methodology unifies all cases of single-input-single-output (SISO) and MIMO systems, as well as minimum-phase and non-minimum-phase systems into one design framework, which lays theoretical fundamental for developing potential DOB design toolbox for a general system. This paper also considers measurement noise, which may severely decrease the DOB's performance. To address this issue, besides the original control channel from disturbance to its estimation error, this paper adds an additional channel when formulating the H_∞ optimization problem. This design methodology is comprehensively analyzed, and applied to a tail-sitter UAV platform that possesses a non-minimum phase angular rate dynamics. Both simulation and experiment show that the designed DOB successfully estimates and suppresses external disturbances in the presence of measurement noise.**

I. Introduction

Disturbance observer (DOB), as an efficient tool for disturbance estimation and compensation for linear systems, has received wide industrial applications, such as hard drives [1], electric bicycles [2], manipulators [3], and UAVs [4]. As shown in Fig. 1, a standard disturbance observer usually consists of a nominal plant inverse G_n^{-1}, which is used to reconstruct plant input and subsequently estimate external disturbance, and a Q filter. The Q filter is designed to (1) customize disturbance estimation frequency range such that the estimate is less contaminated by irrelevant noise; (2) achieve an adequate robust level to modeling errors and uncertainties in nominal plant G_n; and (3) guarantee the causality of DOB (more specifically, $G_n^{-1}Q$). It is worth noting that such a design procedure brings many challenges. (1) The plant inverse for MIMO system is not intuitive as that of SISO systems; (2) The plant inverse has to be stable, which limits the design flexibility for non-minimum phase systems with zeros on the right half complex plane. (3) As

[1]Department of Electronic and Computer Engineering, Hong Kong University of Science and Technology, Hong Kong, China. xlvaa@connect.ust.hk, eefzhang@ust.hk
[2]Department of Mechanical and Aerospace Engineering, University at Buffalo, Buffalo, NY 14260, USA mhzheng@buffalo.edu

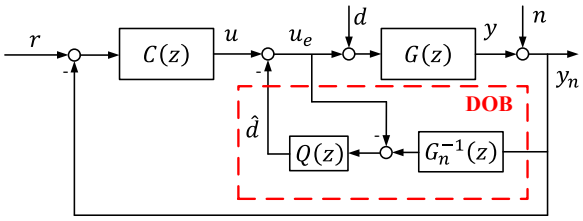

Fig. 1: A general system with conventional DOB

the Q filter has to address multiple issues as mentioned above, its design usually involves considerable tuning work.

Ad-hoc methods have been proposed to address the DOB design for MIMO systems. J. Nie *et. al* [5] ignore the cross channel dynamics and design DOB controllers for each input-output channel separately using conventional DOB design procedures. While this simplification is valid for well decoupled square MIMO systems (i.e., inputs and outputs dimensions are the same), it cannot be generalized to general MIMO systems with noticeable coupling effects. To address this problem, X. Chen *et. al* [6] consider a class of multi-input-single-output (MISO) system and first decouple the nominal system plant model into a form that no cross-channel coupling presents. DOB design on the decoupled system then follow the conventional DOB design procedure for SISO systems.

DOB design for non-minimum phase systems has also gained lots of attention and efforts. X. Chen *et. al* [7] propose a method to design an approximated plant inverse. N. H. Jo *et. al* [8] add a parallel filter to the actual plant, and design the DOB for the augmented system. It is shown that, the augmented system DOB design involves no plant inverse, thus overcomes the restriction of non-minimum phaseness. L. Wang *et. al* [9] propose using the Q filter to cancel unstable poles of the nominal plant inverse, which adds extra restrictions on the Q filter and couples its design with the plant inverse. H. T. Seo *et. al* [10] propose a DOB design methodology for non-minimum phase systems by minimizing H_∞ norm from disturbance to its estimation error. By utilizing H_∞ synthesis techniques based on linear matrix inequality (LMI) convex optimization, the non-minimum phaseness is implicitly treated. As the DOB is designed on open loop system, its stability and optimality when baseline feedback controller presents is, however, not guaranteed. As a result, *ad-hoc* validation and tuning is still required.

Seemingly same efforts have been paid to adopt robust control theory to ease the tunning of Q filter in conventional DOB design, such as [11]–[14]. In [11], the DOB design

problem is transformed into an H_∞ synthesis problem by finding an optimal static output feedback gain for an extended plant. In [12]–[14], the Q-filter is designed through solving an H_∞ optimization problem. More recently, M. Zheng *et. al* [15] propose a DOB design method that minimizes the H_∞ norm of closed-loop dynamics from the disturbance to its estimation error. The design procedure does not require an explicit plant inverse nor tunning on the Q filter. Compared to the previous work based on H_∞ synthesis, this method provides a more complete and systematic treatment by synthesizing both the plant inverse G_n^{-1} and Q filter as well as taking into account the baseline feedback controller. The synthesized DOB is therefore guaranteed to be optimal and stable.

This paper extends the work in [15], which is primarily concerned with MIMO systems, to non-minimum phase systems. This paper verifies the proposed DOB design methodology for non-minimum phase systems, provides the solvability proof of such an approach by using results from linear matrix inequality (LMI) based H_∞ synthesis [16]. Furthermore, a second channel is added in addition to the original channel from disturbance to its estimation error proposed in [15] to address measurement noise. The proposed DOB design methodology produces an optimal and stable DOB with enhanced disturbance and noise attenuation, and meanwhile eliminates all the human design efforts on the Q filter and plant inverse, which is rather challenging for MIMO or non-minimum phase systems. Instead, the human design efforts are all shifted to tune the proper weighting functions associated with measurement noise and disturbance, which is quite intuitive and uniform across almost all linear systems (particularly, MIMO and non-minimum phase systems).

As the DOB can essentially be viewed as a part of the feedback controller, one may wonder why not design the entire feedback controller by H_∞ synthesis at the beginning, such that the designed feedback controller achieves similar disturbance attenuation to the DOB. While such equivalence is mathematically true, separating the DOB from the baseline controller design gives us more freedom in actual implementation. For example, the DOB, running as an add-on to the baseline controller, can estimate the disturbance in real time. One can also easily turn on/off the add-on DOB at different situations, where high disturbance attenuation is not necessary.

The remainder of the paper is organized as follows: Section II formulates the DOB design problem into an H_∞ optimization problem; Section III applies the proposed DOB onto a tail-sitter UAV platform; The simulation results in time domain and experiment verification will be separately introduced in Section IV and Section V, respectively; Section VI concludes the paper.

II. H_∞ BASED DOB DESIGN

This section formulates the DOB design problem into an H_∞ optimization problem based on robust control theory.

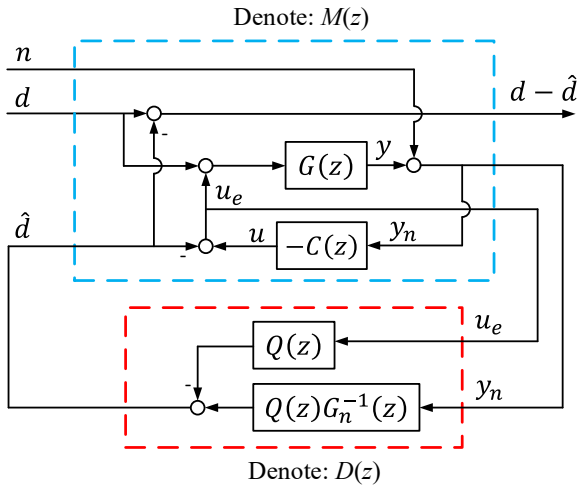

Fig. 2: Equivalent representation for the system in Fig. 1

Define $T_f(z)$ as the transfer function from d to $(d-\hat{d})$, i.e.,

$$d - \hat{d} = T_f(z)d \tag{1}$$

From the system interconnections shown in Fig. 1, one can obtain

$$T_f = 1 - \frac{Q[G_n^{-1}G + GC][1 + GC]^{-1}}{(1-Q) + Q[G_n^{-1}G + GC][1 + GC]^{-1}} \tag{2}$$

When designing a DOB for an actual system subject to disturbances and noises, we ultimately want the disturbance estimation error $d-\hat{d}$ to be zero over all possible disturbance and noise, or equivalently, minimizing the H_∞ norm of transfer function from disturbance and noise to disturbance estimation error $d-\hat{d}$. As shown in Fig. 2, the optimization problem is

$$\min_{D(z)} \ \|F_l(M(z), D(z))\|_\infty \tag{3}$$

where $M(z)$ denotes the baseline feedback control loop, $D(z)$ denotes the DOB to be designed, and $F_l(M(z), D(z)) = M_{11} + M_{12}D(I - M_{22}D)^{-1}M_{21}$ represents the closed loop transfer function from exogenous inputs (d and n) to output $d - \hat{d}$.

Let the state space realization of $G(z)$ be (A_p, B_p, C_p) and $-C(z)$ be (A_c, B_c, C_c, D_c), all are minimal realization, then

$$\begin{aligned} x_p(k+1) &= A_p x_p(k) + B_p(u_e(k) + d(k)) \\ y(k) &= C_p x_p(k) \end{aligned} \tag{4}$$

and

$$\begin{aligned} x_c(k+1) &= A_c x_c(k) + B_c y_n(k) \\ u(k) &= C_c x_c(k) + D_c y_n(k) \end{aligned} \tag{5}$$

Then, the system $M(z)$ has the state-space realization as

below

$$\begin{aligned}
\underbrace{\begin{bmatrix} x_p(k+1) \\ x_c(k+1) \end{bmatrix}}_{x(k+1)} &= \underbrace{\begin{bmatrix} A_p + B_p D_c C_p & B_p C_c \\ B_c C_p & A_c \end{bmatrix}}_{A} \underbrace{\begin{bmatrix} x_p(k) \\ x_c(k) \end{bmatrix}}_{x(k)} \\
&\quad + \underbrace{\begin{bmatrix} B_p & B_p D_c \\ 0 & B_c \end{bmatrix}}_{B_1} \begin{bmatrix} d(k) \\ n(k) \end{bmatrix} + \underbrace{\begin{bmatrix} -B_p \\ 0 \end{bmatrix}}_{B_2} \hat{d}(k) \\
d(k) - \hat{d}(k) &= \underbrace{\begin{bmatrix} 0 & 0 \end{bmatrix}}_{C_1} \underbrace{\begin{bmatrix} x_p(k) \\ x_c(k) \end{bmatrix}}_{x(k)} + \underbrace{\begin{bmatrix} I & 0 \end{bmatrix}}_{D_{11}} \begin{bmatrix} d(k) \\ n(k) \end{bmatrix} \\
&\quad - \hat{d}(k) \\
\begin{bmatrix} y_n(k) \\ u_e(k) \end{bmatrix} &= \underbrace{\begin{bmatrix} C_p & 0 \\ D_c C_p & C_c \end{bmatrix}}_{C_2} \underbrace{\begin{bmatrix} x_p(k) \\ x_c(k) \end{bmatrix}}_{x(k)} \\
&\quad + \underbrace{\begin{bmatrix} 0 & I \\ 0 & D_c \end{bmatrix}}_{D_{21}} \begin{bmatrix} d(k) \\ n(k) \end{bmatrix} + \underbrace{\begin{bmatrix} 0 \\ -I \end{bmatrix}}_{D_{22}} \hat{d}(k)
\end{aligned} \tag{6}$$

Or in a more compact form,

$$\begin{aligned}
\dot{x} &= Ax + B_1 \begin{bmatrix} d \\ n \end{bmatrix} + B_2 \hat{d} \\
d - \hat{d} &= C_1 x + D_{11} \begin{bmatrix} d \\ n \end{bmatrix} + D_{12} \hat{d} \\
\begin{bmatrix} y_n \\ u_e \end{bmatrix} &= C_2 x + D_{21} \begin{bmatrix} d \\ n \end{bmatrix} + D_{22} \hat{d}
\end{aligned} \tag{7}$$

Then, by [16], the standard H_∞ synthesis problem in (3) is solvable if (A, B_2, C_2) is both detectable and stabilizable (see assumption (**A1**) in [16]), which is clearly true as the baseline feedback controller always stabilizes the system plant (i.e. the closed loop system matrix A is stable).

Weighting filters: In general, minimizing the estimation error over both disturbances and noises on entire frequency domain is not possible and usually produces impractical feedback controller. Noting that the disturbances and noises are usually distributed on different frequency range, i.e, the disturbances are usually on low frequency range while the noise on high frequency range, we can add two weighting filters W_d and W_n to respectively re-weight the cost from disturbances and noise to the estimation error over different frequencies. Define

$$W(z) = \begin{bmatrix} W_n(z) & 0 \\ 0 & W_d(z) \end{bmatrix} \tag{8}$$

The DOB synthesis becomes

$$\min_{D(z)} \ \|F_l(M(z), D(z))W(z)\|_\infty \tag{9}$$

The system interconnections with weighting filters are shown in Fig. 3. From our previous formulation, we did not make any assumption on the dimension or minimum phaseness of the system plant. The system dimensions and non-minimum phaseness of the system are implicitly treated by the H_∞ solver using linear matrix inequality (LMI) constraints [16]. The synthesized controller $D(z)$ (the disturbance observer) would minimize the corresponding H_∞

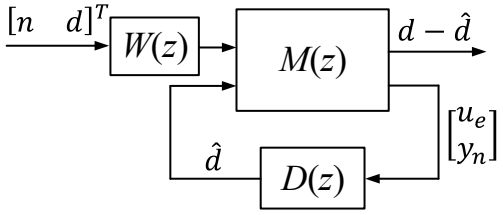

Fig. 3: DOB synthesis in LFT form

norm while guarantee both the casualty and the closed loop stability. After obtaining the optimal $D(z)$, one can immediately compute the $Q(z)$ filter in the conventional DOB by $Q(z) = D_1(z)$, and the plant inverse $G_n^{-1}(z)$ as $G_n^{-1}(z) = D_1^{-1}(z)D_2(z)$.

III. Application to a Tail-Sitter UAV

Convertible vertical take-off and landing (VTOL) unmanned aerial vehicles (UAVs), which combines the maneuverability of a rotary-wing aircraft and the high level flight efficiency of a fixed-wing aircraft, attracts much attention recently [17]–[19]. Especially the tail-sitter VTOL UAVs, which possess high control authority and with simple mechanical structure, become quite promising. A main drawback of tail-sitters is that they are rather sensitive to cross wind during hover flight, due to their large wing area. In this paper, we verify the effectiveness of the proposed DOB design method by applying it to the attitude control of such tail-sitter UAVs [20].

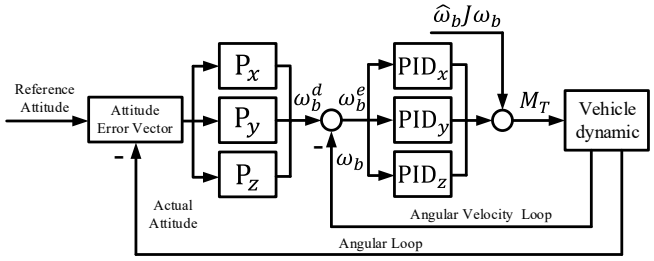

Fig. 4: Attitude controller diagram

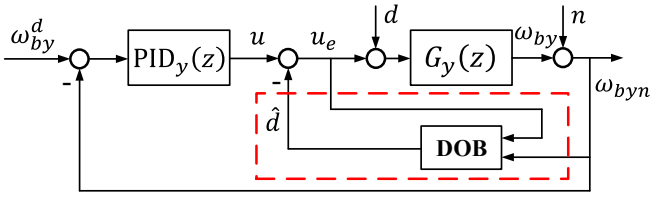

Fig. 5: Angular velocity loop in pitch direction with DOB module

In our previous work [21], we have developed a cascaded attitude controller as shown in Fig. 4, using the *Quaternion Linear* method. Consequently, the roll, pitch, and yaw directions can be controlled separately. For simplicity, we will take the pitch direction as an example to demonstrate the DOB design process. During the hovering flight, the

gyroscopic effect (i.e., the $\hat{\omega}_b J \omega_b$ term) of the vehicle is a very small quadratic term and can, therefore, be ignored. The angular velocity loop in pitch direction with DOB module is shown in Fig. 5. $\text{PID}_y(z)$ is the baseline angular velocity controller being used, $G_y(z)$ is the system plant from the input $u_e + d$ to angular velocity ω_{by}.

Ideally, the relationship between moment and angular velocity is an integrator, i.e, $J_{yy}\dot{\omega}_{by} = M_{Ty}$. The corresponding transfer function is

$$\frac{\omega_{by}(z)}{M_{Ty}(z)} = \frac{\triangle t}{J_{yy}(z-1)} \tag{10}$$

where $\triangle t = 0.004$ s (the attitude loop runs at 250 Hz).

However, as the UAV body and motor arms are not strictly rigid, there exist flexible modes in $G_y(z)$. Other factors such as motor dynamics, controller delay, aerodynamic damping, will also cause the actual dynamic model $G_y(z)$ far more complicated than an integral action in (10). In practice, we identify the vehicle's angular velocity dynamic model in the frequency domain by frequency sweep methods. The identified system frequency response is shown in Fig. 6. It is seen that at the frequency range from 4 to 50 rad/s, there is an integral mode corresponding to our first principle integral model, while at the high frequency range from 50 to 600 rad/s, there are three flexible modes.

As the bandwidth of the baseline feedback controller is well below the flexible modes, we can reasonably ignore it to simplify the DOB design. As a result, we perform the system identification on our simulated platform presented in [22], which captures many details of the actual VTOL UAV dynamics including motor saturation, delay, aerodynamic force and moments, etc., but not flexible modes. As shown later, the designed DOB based on the simulated model turned out to work for the real system surprisingly well. Based on the frequency response data obtained in the simulator, the fitted transfer function is

$$G_y(z) = \frac{0.14131(z+1.716)}{(z-1)(z-0.9447)} \tag{11}$$

where $z = -1.716$ is an unstable zero, which implies $G_y(z)$ is a non-minimum phase system.

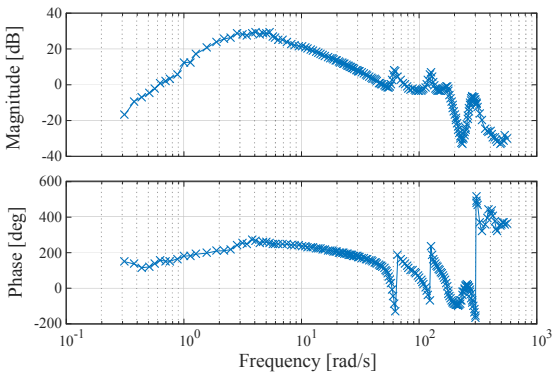

Fig. 6: System identification in pitch direction

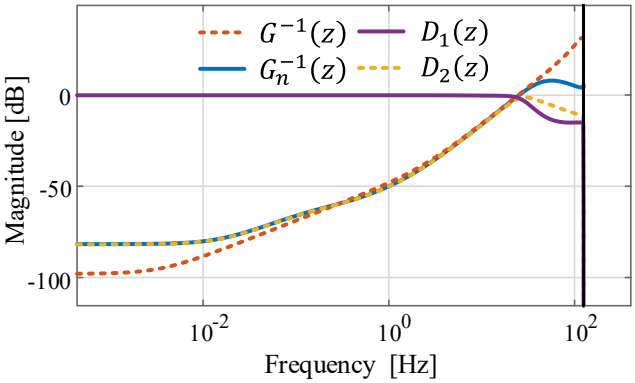

Fig. 7: DOB design results

The baseline feedback PID controller is designed as

$$\text{PID}_y(z) = \frac{0.9002(z-0.8343)(z-0.9987)}{z(z-1)} \tag{12}$$

In our considered scenario, the disturbance is usually caused by cross wind, which is typically concentrated on low frequency range, while the measurement noise is usually at high frequency range. According to the practical demands, the weighting functions are respectively designed as

$$\begin{aligned} W_n &= \frac{3.7584(z-0.9949)}{(z+0.925)} \\ W_d &= \frac{0.19908(z+0.8997)}{(z-0.9962)} \end{aligned} \tag{13}$$

With the knowledge of $G(z)$, $C(z)$ and $W(z)$, the DOB can be synthesis by solving (9). The designed results are shown in Fig. 7. As we can see, $G_n^{-1}(z)$ matches $G^{-1}(z)$ quite well from 0.1 Hz to 25 Hz, the Q filter is a typical low pass filter as expected. Fig. 8 shows the bode diagram from d to $\hat{d}$, which indicates the designed DOB can estimate the magnitude of the disturbance up to 25 Hz.

Fig. 9 shows the bode diagram from the disturbance d to plant output ω_{byn}. It can be seen that, below 10 Hz,

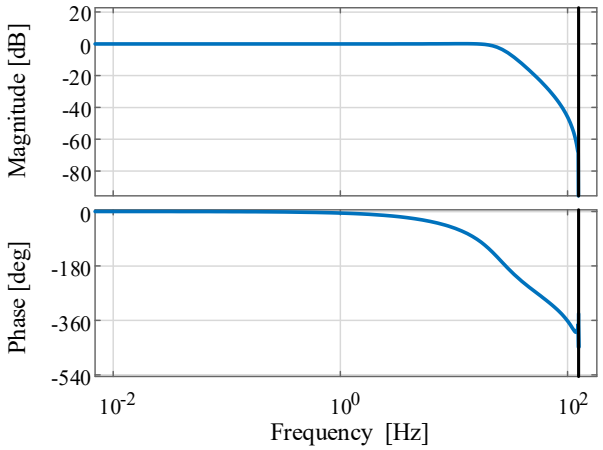

Fig. 8: Bode diagram from d to $\hat{d}$

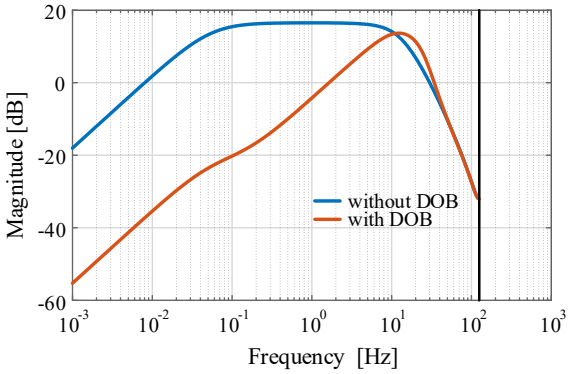

Fig. 9: Bode diagram from d to plant output ω_{byn}

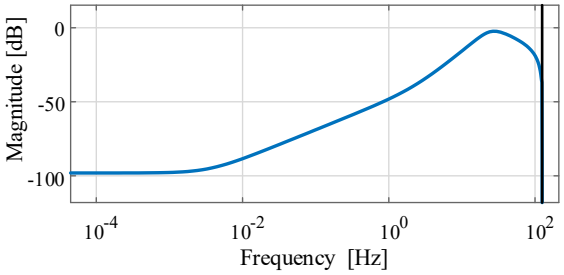

Fig. 10: Bode diagram from n to $\hat{d}$

the added DOB module can effectively attenuate the effects from disturbance, which dramatically improve the control performance. Fig. 10 shows the bode diagram from the measurement noise n to disturbance d. It is seen that the magnitude of the transfer function from noise to disturbance estimate is well below 0 dB throughout the entire frequency range. This indicates that the measurement noise shows negligible effects on the DOB output.

IV. Simulation Results

We apply the same design procedure to roll and yaw directions of the UAV attitude control. The designed DOB were all implemented in our simulation platform with simulated disturbances and measurement noise. Comparison study with DOB turned on and off were conducted and shown in Fig. 11 and Fig. 12, respectively. The maximum attitude error in pitch, roll, and yaw direction with DOB turned off are respectively 0.12 rad, 0.15 rad, and 0.12 rad with DOB turned off, and 0.01 rad, 0.02 rad, and 0.02 rad, respectively, with DOB turned on. In the simulation, the disturbance d is produced by filtering a serial of random value with a low pass filter (1 Hz cutoff frequency). The resulting disturbance added to the system and the disturbance estimation are shown in Fig. 13. It is seen that the estimated disturbance tracks the actual disturbance quite well. Finally, Fig 14 shows the added measurement noise in our simulation. The noise is a white Gaussian noise with the power of -68 dBW, which is characterized by the actual sensor measurements in our UAV platform.

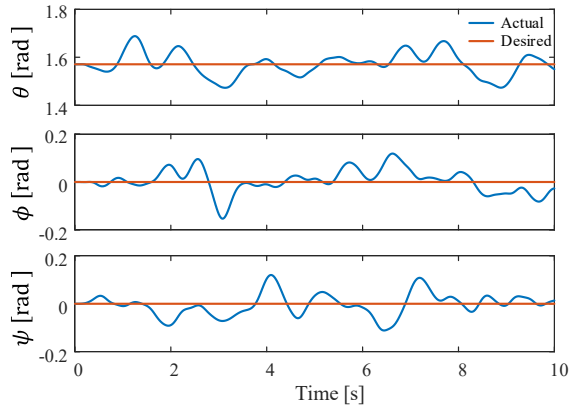

Fig. 11: Attitude with DOB turned off

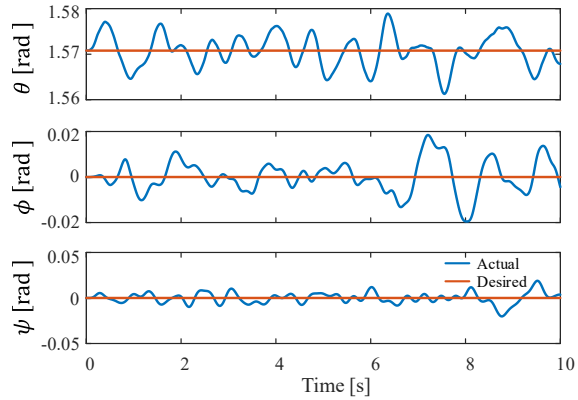

Fig. 12: Attitude with DOB turned on

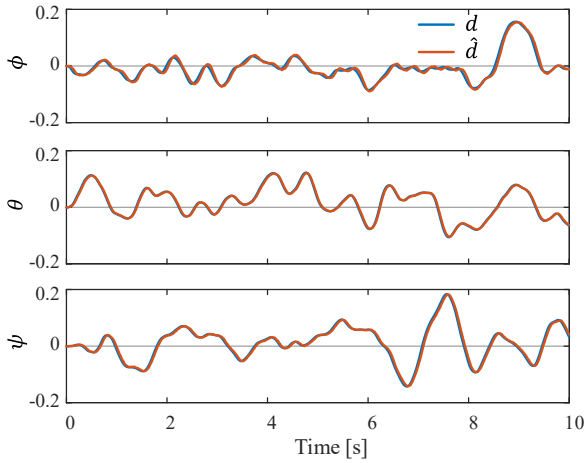

Fig. 13: Disturbance added to the system and the disturbance estimated by DOB along x_b, y_b, and z_b direction.

V. Experiment Verification

The experiment verification was conducted on our attitude testing platform. Due to the mechanical restrictions of the UAV platform, we can only conduct the test on body z axis (or roll direction at hovering), as shown in Fig. 15. A freely rotatable rod is rigidly connected to the UAV body, such that the vehicle can rotate along its body z axis (the body frame

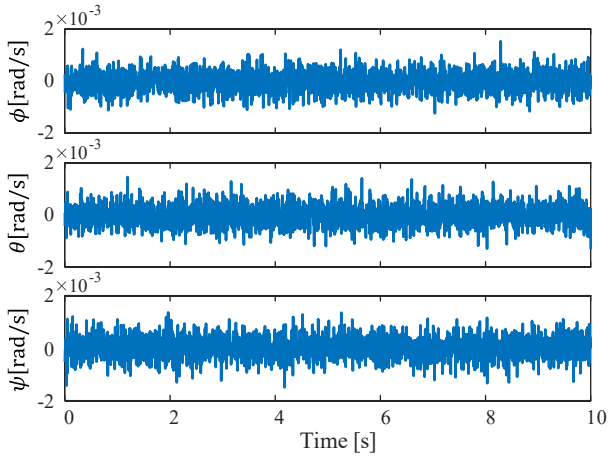

Fig. 14: Measurement noise added in the simulation

takes convention from fixed-wing aircraft where the x axis points front, y axis points right and z axis points down at level flight). A rubber band is connected to the UAV wingtip to produce a moment disturbance.

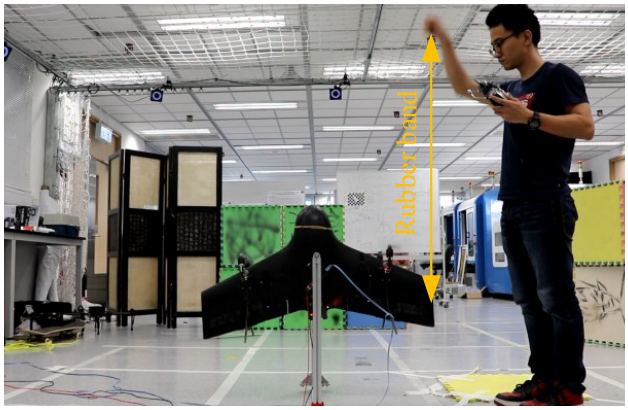

Fig. 15: Experiment setup (video available at `https://youtu.be/QsALotADWck`)

The test results are shown in Fig. 16. As shown in Fig. 16 (a), at 11.3 s, we started pulling the rubber band at approximately 1 Hz of frequency. The disturbance magnitude was gradually increased by pulling the rubber band to different locations. With this artificially produced disturbances, the comparison experiments with the DOB turned on and off were done. As we can see from Fig. 16 (a), from 49 s to 62 s, the maximum attitude error is around 0.3 rad with the DOB turned off. However, from 64 s to 77 s with similar external disturbance, the maximum attitude error reduces to 0.08 rad with the DOB turned on. Fig. 16 (b) shows the angular velocity tracking performance with DOB turned on and off. It can be seen that the desired value can be well tracked with the DOB turned on (refer to the zoom in drawing from 44 s to 47 s), however, with the DOB turned off, there exists an offset due to the external disturbance. Fig. 16 (c) shows the estimated disturbance from the designed DOB. Due to the lack of ground truth external disturbance, we cannot evaluate its estimation accuracy. But the figure does show a sinusoidal

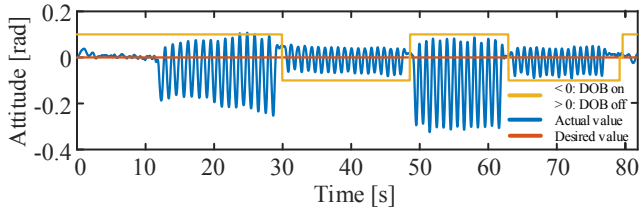

(a) Vehicle attitude with DOB turned on/off

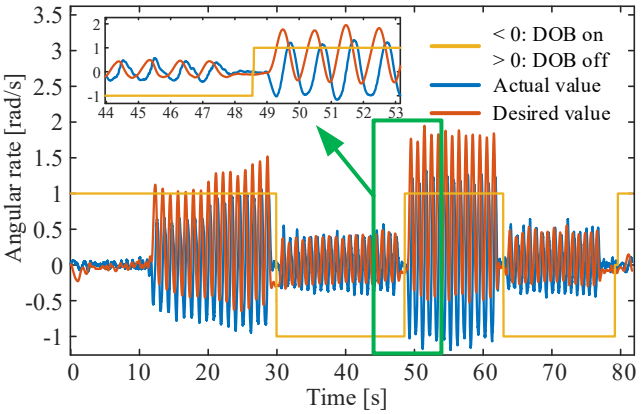

(b) Vehicle angular velocity with DOB turned on/off

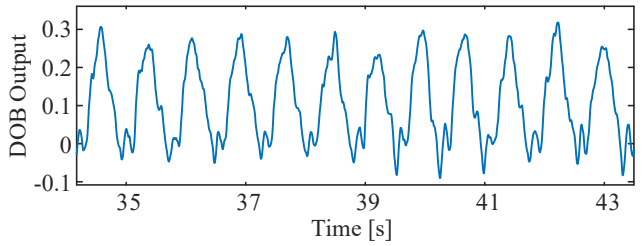

(c) Estimated disturbance during the experiment

Fig. 16: Experiment results

shape disturbances that agree with the actual experiments.

VI. Conclusion and Future Work

In this paper, a general DOB design method for linear systems with multi-inputs, multi-outputs and non-minimum phaseness has been proposed. The proposed DOB minimizes the weighted H_∞ norm of the baseline feedback loop from the disturbance and measurement noise to the disturbance estimate error. Through adjusting the disturbance weighting function and noise weighting function, one can design a DOB with sufficient large attenuation on both disturbances and noises. The use of H_∞ synthesis techniques enable the system dimension and non-minimum phaseness to be implicitly treated in linear matrix inequality (LMI) constraints. The synthesized DOB is guaranteed to be causal, stable as well as optimal. A detailed evaluation was performed on a tail-sitter VTOL UAV platform. Both simulation and experiments were conducted to verify the effectiveness of the DOB design method. Future work will focus on robust DOB design with consideration of model uncertainty.

REFERENCES

[1] Q. W. Jia, "Disturbance rejection through disturbance observer with adaptive frequency estimation," *IEEE Transactions on Magnetics*, vol. 45, no. 6, pp. 2675–2678, 2009.

[2] X. Fan and M. Tomizuka, "Robust disturbance observer design for a power-assist electric bicycle," in *American Control Conference (ACC), 2010*. IEEE, 2010, pp. 1166–1171.

[3] J. N. Yun and J.-B. Su, "Design of a disturbance observer for a two-link manipulator with flexible joints," *IEEE Transactions on Control Systems Technology*, vol. 22, no. 2, pp. 809–815, 2014.

[4] S. J. Lee, S. Kim, K. H. Johansson, and H. J. Kim, "Robust acceleration control of a hexarotor uav with a disturbance observer," in *2016 IEEE 55th Conference on Decision and Control (CDC)*. IEEE, 2016, pp. 4166–4171.

[5] J. Nie and R. Horowitz, "Design and implementation of dual-stage track-following control for hard disk drives," in *Proceedings of ASME 2nd Dynamic Systems and Control Conference, Hollywood, CA, Oct*, 2009, pp. 12–14.

[6] X. Chen and M. Tomizuka, "Optimal decoupled disturbance observers for dual-input single-output systems," *Journal of Dynamic Systems, Measurement, and Control*, vol. 136, no. 5, p. 051018, 2014.

[7] X. Chen, G. Zhai, and T. Fukuda, "An approximate inverse system for nonminimum-phase systems and its application to disturbance observer," *Systems & Control Letters*, vol. 52, no. 3, pp. 193–207, 2004.

[8] N. H. Jo, H. Shim, and Y. I. Son, "Disturbance observer for non-minimum phase linear systems," *International Journal of Control, Automation and Systems*, vol. 8, no. 5, pp. 994–1002, 2010.

[9] L. Wang and J. Su, "Disturbance rejection control for non-minimum phase systems with optimal disturbance observer," *ISA transactions*, vol. 57, pp. 1–9, 2015.

[10] H. T. Seo, K. S. Kim, and S. Kim, "Generalized design of disturbance observer for non-minimum phase system using an h-infinity approach," in *International Conference on Control, Automation and Systems (ICCAS)*. IEEE, 2013, pp. 1–4.

[11] C.-C. Wang and M. Tomizuka, "Design of robustly stable disturbance observers based on closed loop consideration using h/sub/spl infin//optimization and its applications to motion control systems," in *American Control Conference, 2004. Proceedings of the 2004*, vol. 4. IEEE, 2004, pp. 3764–3769.

[12] C. Thum, C. Du, F. Lewis, B. Chen, and E. Ong, "H disturbance observer design for high precision track following in hard disk drives," *IET control theory & applications*, vol. 3, no. 12, pp. 1591–1598, 2009.

[13] J. Su, L. Wang, and J. Yun, "A design of disturbance observer in standard h control framework," *International Journal of Robust and Nonlinear Control*, vol. 25, no. 16, pp. 2894–2910, 2015.

[14] C. Du, H. Li, C. Thum, F. Lewis, and Y. Wang, "Simple disturbance observer for disturbance compensation," *IET control theory & applications*, vol. 4, no. 9, pp. 1748–1755, 2010.

[15] M. Zheng, S. Zhou, and M. Tomizuka, "A design methodology for disturbance observer with application to precision motion control: An h-infinity based approach," in *American Control Conference (ACC), 2017*. IEEE, 2017, pp. 3524–3529.

[16] P. Gahinet and P. Apkarian, "A linear matrix inequality approach to h control," *International journal of robust and nonlinear control*, vol. 4, no. 4, pp. 421–448, 1994.

[17] A. S. Saeed, A. B. Younes, S. Islam, J. Dias, L. Seneviratne, and G. Cai, "A review on the platform design, dynamic modeling and control of hybrid UAVs," in *2015 International Conference on Unmanned Aircraft Systems (ICUAS)*. IEEE, 2015, pp. 806–815.

[18] H. Gu, X. Lyu, Z. Li, S. Shen, and F. Zhang, "Development and experimental verification of a hybrid vertical take-off and landing (vtol) unmanned aerial vehicle (uav)," in *2017 International Conference on Unmanned Aircraft Systems (ICUAS)*. IEEE, 2017, pp. 160–169.

[19] Y. Wang, X. Lyu, H. Gu, S. Shen, Z. Li, and F. Zhang, "Design, implementation and verification of a quadrotor tail-sitter vtol uav," in *2017 International Conference on Unmanned Aircraft Systems (ICUAS)*. IEEE, 2017, pp. 462–471.

[20] X. Lyu, H. Gu, Y. Wang, Z. Li, S. Shen, and F. Zhang, "Design and implementation of a quadrotor tail-sitter vtol uav," in *2017 IEEE International Conference on Robotics and Automation (ICRA)*. IEEE, 2017, pp. 3924–3930.

[21] X. Lyu, H. Gu, J. Zhou, Z. Li, S. Shen, and F. Zhang, "A hierarchical control approach for a quadrotor tail-sitter vtol uav and experimental verification," in *2017 IEEE/RSJ International Conference on Intelligent Robots and Systems (IROS)*. IEEE, 2017 (to appear).

[22] F. Zhang, X. Lyu, Y. Wang, H. Gu, and Z. Li, "Modeling and flight control simulation of a quadrotor tailsitter vtol uav," in *AIAA Modeling and Simulation Technologies Conference*, 2017, p. 1561.